

Site Diversity in Downlink Optical Satellite Networks Through Ground Station Selection

Eylem Erdogan, *Member, IEEE*, Ibrahim Altunbas, *Senior Member, IEEE*, Gunes Kurt, *Senior Member, IEEE*, Michel Bellemare, Guillaume Lamontagne, Halim Yanikomeroglu, *Fellow, IEEE*

Abstract—Recent advances have shown that satellite communication (SatCom) will be an important enabler for next generation terrestrial networks as it can provide numerous advantages, including global coverage, high speed connectivity, reliability, and instant deployment. An ideal alternative for radio frequency (RF) satellites is its free-space optical (FSO) counterpart. FSO or laser SatCom can mitigate the problems occurring in RF SatCom, while providing important advantages, including reduced mass, lower consumption, better throughput, and lower costs. Furthermore, laser SatCom is inherently resistant to jamming, interception, and interference. Owing to these benefits, this paper focuses on downlink laser SatCom, where the best ground station (GS) is selected among numerous candidates to provide reliable connectivity and maximum site diversity. To quantify the performance of the proposed scheme, we derive closed-form outage probability and ergodic capacity expressions for two different practical GS deployment scenarios. Furthermore, asymptotic analysis is conducted to obtain the overall site diversity gain, and aperture averaging is studied to illustrate the impact of aperture diameter on the overall performance. Finally, important design guidelines that can be useful in the design of practical laser SatComs are outlined.

Index Terms—Laser satellite communication, site diversity, free-space optical communication, atmospheric turbulence and attenuation.

I. INTRODUCTION

Satellite communication (SatCom) has become an important part of aerial networks in recent years due to its capabilities, which include flawless wireless connectivity, wide service coverage, and high-fidelity services for all the users around the world. An important feature of SatCom is to simultaneously transfer the signal rapidly around the Earth by providing distance-insensitive point-to-multipoint communications [1]. So far, satellites have been used for television coverage, data communication, navigation, weather forecasts, climate and environmental monitoring, space science, and so on [2]. Satellites can be divided into three main categories depending on their altitudes and orbit types, low Earth orbit (LEO), medium Earth

orbit (MEO) and geostationary Earth orbit (GEO). GEO satellites are located at about 36000 km above the Earth's equator to provide wide coverage, whereas LEO satellites, which circle around the Earth at lower altitudes, have faster rotations, require less power, and are cheaper than GEO and MEO satellites [3]. The technology behind SatCom is mainly based on radio-frequency (RF) systems, where 100 MHz to 50 GHz frequencies are used depending on the types and applications of satellites. In recent years, SatCom has emerged to provide high-speed, seamless broadband Internet connectivity around the globe as many different companies have started to launch constellations of satellites. For instance, SpaceX's Starlink recently began launching LEO satellites operating at high frequencies, above 24 GHz [4]. Similarly, OneWeb is planning to launch more than 600 LEO satellites in 2020, which will operate in the 12 to 18 GHz frequency range [5]. These recent developments suggest that RF-SatCom will become a key enabler in the integration of aerial and terrestrial networks in future wireless communication systems. In RF-SatCom, the most important drawbacks are cost and regulatory restrictions, as it requires high data rates and broader bandwidths to connect anyone at anytime. Furthermore, RF-SatCom is prone to interference, jamming, and interception, which pose security risks, especially for military communications.

As a solution to these problems, free-space optical (FSO) or laser SatCom has attracted considerable interest both in recent academic and industry publications [6]. In laser SatCom, 20 to 375 THz spectrum¹ can be used to provide very high throughput in satellite-to-ground (downlink) and ground-to-satellite (uplink) communications [7]. Laser SatCom can also provide significant advantages compared to its RF counterpart, including smaller antennas, reduced mass, lower consumption, better throughput, and lower costs. Furthermore, the narrow beam used in optical systems can provide secure communication, and it is immune to jamming, interception, interference. In addition, laser SatCom does not need regulatory restrictions for frequency use due to its inherent nature [8]. Due to these advantages, laser SatCom is expected to become a key enabler for future optical satellite systems, particularly for satellite-to-ground (downlink) communications, where line-of-sight (LOS) connectivity can be established perfectly [9]. In downlink laser SatCom, the major adverse effects are atmospheric turbulence, atmospheric attenuation, and angle of arrival (AoA) fluctuations [7]. The latter can be attenuated

E. Erdogan is with the Department of Electrical and Electronics Engineering, Istanbul Medeniyet University, 34700, Uskudar, Istanbul, Turkey.

I. Altunbas and Gunes Kurt are with the Department of Electronics and Communication Engineering, Istanbul Technical University, 34469, Maslak, Istanbul, Turkey.

G. Kurt is also with the Department of Systems and Computer Engineering, Ottawa, K1S 5B6, ON, Canada

Michel Bellemare and Guillaume Lamontagne are with the MDA Corporation, Sainte-Anne-de-Bellevue, Québec, H9X 3R2, QC, Canada

H. Yanikomeroglu is with the Department of Systems and Computer Engineering, Carleton University, Ottawa, K1S 5B6, ON, Canada.

This work was supported in part by the Optical Satellite Communications Consortium Canada (OSC).

¹In laser SatCom, only a small portion of the frequency spectrum can be used due to huge atmospheric losses.

by using variable-focus lenses, which can adjust the beam size [10]. Also, aperture averaging, where the scintillation is spatially averaged over the aperture, can be used to reduce the adverse effects of atmospheric turbulence [11]. Finally, atmospheric attenuation due to adverse weather conditions can be resolved by achieving site diversity through multiple GSs [12]–[15]. It can also be resolved by attaining spatial diversity with the aid of multiple apertures on a single GS, using appropriate combining techniques, such as selection combining, maximum ratio combining or equal gain combining [16], [17].

Due to the advantages outlined above, optical satellites have become an important topic in the recent literature. In [18]–[21], the issue of optical ground-to-satellite (uplink) communication was considered, and important performance metrics, including outage probability, error probability, and link capacity, were obtained in the presence beam wandering, climatic effects, and atmospheric attenuation. By contrast, [16] and [22] focused on downlink SatCom, where the former investigated the impact of spatial diversity and aperture averaging, and the latter examined the throughput. Furthermore, [23] and [24] proposed using FSO communication as a feeder link where the ground station (GS) feeds the satellite through a high capacity link.

In this paper, we pursue a different line of inquiry by providing a detailed analysis for the downlink optical SatCom systems, where the best GS that provides the best channel conditions is selected among a number of GSs to achieve maximum site diversity and to deal with the adverse weather conditions. It is important to note that site diversity, which can be crucial for creating seamless connectivity between satellite-to-ground links, has already been discussed in the literature e.g., [12]–[15] and the references therein. However, these previous works focused on the optimum GS selection problem from the network layer point-of-view. To the best of our knowledge, none of these works have considered the physical layer performance of the optical SatCom with GS selection. Given the importance of site diversity, and to fill the gap in the literature, we focus on the physical layer performance of the downlink optical SatCom with multiple GSs². To quantify the performance of the proposed setup, we consider an aggregate channel model consisting of atmospheric turbulence and atmospheric attenuation, where we obtained two performance indicators, outage probability and ergodic capacity. More precisely, the paper makes the following specific contributions:

- We focus on the physical layer performance of the downlink optical SatCom, where the best GS is selected among a set of \mathcal{K} sites that are available for communication, to minimize the outage probability and to maximize the ergodic capacity. For this network, we consider an aggregate channel model consisting of turbulence induced fading, and atmospheric attenuation due to Mie scattering and geometrical scattering, and we obtain the instantaneous signal-to-noise ratio (SNR).

- After obtaining the instantaneous SNR, we derive new closed-form outage probability and ergodic capacity expressions to characterize the overall performance of the proposed scheme. We further elaborate the system at high SNR to obtain the site diversity gain.
- We provide two new GS deployment scenarios: ground level deployment and high ground windy weather deployment. We also provide some interesting system design guidelines and consider aperture averaging to mitigate the adverse effects of turbulence induced fading.

The remainder of the paper is organized as follows: In Section II, the system model and problem formulation are outlined. In Section III, the outage probability and ergodic capacity analyses are presented, and the site diversity gain is obtained. In Section IV, numerical results are provided, and Section V concludes the paper.

II. SYSTEM MODEL AND PROBLEM FORMULATION

We consider here a downlink optical SatCom where a low Earth orbit (LEO) satellite deployed at an altitude of 500 km seeks to communicate with the best GS selected among a set of \mathcal{K} sites that are available for communication, as depicted in Fig. 1. In the proposed model, the best GS with the highest signal-to-noise (SNR) ratio is selected to enhance the system performance by creating site diversity [25]. Prior to the data transmission, the satellite, which is moving at a speed of 7 km/s, takes aim at the best GS, and the GS is aligned with the incoming beam to compensate for the bore-sight pointing errors. In this setup, the aggregated channel model is taken into consideration which consists of atmospheric attenuation $(I_j^{(a)})_{j=1}^{\mathcal{K}}$ and turbulence induced fading $(I_j^{(r)})_{j=1}^{\mathcal{K}}$. Mathematically speaking, the aggregated channel of the j -th GS can be expressed as

$$I_j = I_j^{(a)} I_j^{(r)}, \quad (1)$$

and the instantaneous SNR (γ_j) can be expressed as

$$\gamma_j = \left(\frac{P_S}{N_0} I_j^2 \right), \quad (2)$$

where P_S is the power of the satellite, and N_0 is the one sided noise power spectral density. The following subsections present the atmospheric attenuation and turbulence induced fading models for the proposed model.

A. Atmospheric Attenuation Model

In downlink optical SatCom, two different scattering effects can be observed as the beam propagates to the GS. The first is Mie scattering, which redirects the transmitted signal from its intended direction when the signal wavelength is equal to the diameter of the particles in the medium. The second is geometrical scattering, which causes reflection, refraction, and scattering when the size of the particles in the medium is much greater than the signal wavelength³.

²In the proposed setup, we assume that all GSs are connected through fibre-optic wires, and the GS with the highest communication reliability can share the information to the other GSs.

³It is important to note that Rayleigh scattering may also adversely affect the optical SatCom. However, it can be negligible for systems operating below 375 THz, as per the ITU-R report [7].

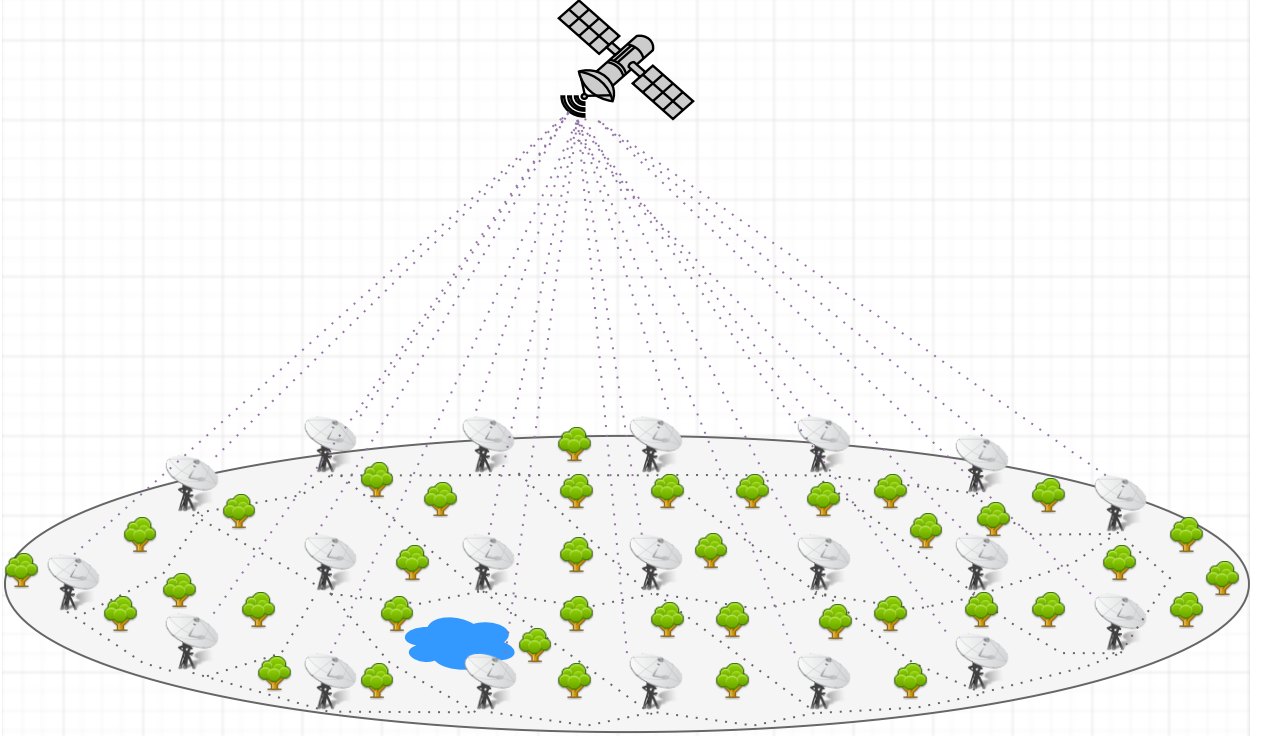


Fig. 1: Optical downlink SatCom with multiple ground stations.

1) *Atmospheric Attenuation Due to Mie Scattering:* Mie scattering is specified as the primary source of losses in downlink optical SatCom operating between 150 and 375 THz frequencies ($\lambda = 0.8 - 2 \mu\text{m}$) and it is largely caused by microscopic particles of water [7, Sec. (3.1)]. The following expression, which can precisely model the Mie scattering effects, is appropriate for GSs located at altitudes between 0 and 5 km above the mean sea level [7]:

$$\rho' = ah_E^3 + bh_E^2 + ch_E + d, \quad (3)$$

where ρ' denotes the extinction ratio, h_E stands for the height of the ES above the mean sea level (km), and a , b , c and d are the wavelength λ (μm)-dependent empirical coefficients, which can be expressed as

$$\begin{aligned} a &= -0.000545\lambda^2 + 0.002\lambda - 0.0038 \\ b &= 0.00628\lambda^2 - 0.0232\lambda + 0.0439 \\ c &= -0.028\lambda^2 + 0.101\lambda - 0.18 \\ d &= -0.228\lambda^3 + 0.922\lambda^2 - 1.26\lambda + 0.719, \end{aligned} \quad (4)$$

and the atmospheric attenuation due to Mie scattering ($I_j^{(m)}$) can be expressed as⁴

$$I_j^{(m)} = \exp\left(-\frac{\rho'}{\sin(\theta_j)}\right), \quad (5)$$

where θ_j is the elevation angle of the j -th GS.

⁴Throughout the paper, we assume that the height of each GS above the mean sea level is the same. We also assume that all GSs are propagating at the same wavelength. However, the elevation angles and the propagation distances may vary depending on the location of each GS.

TABLE I: Geometrical scattering parameters for various types of clouds at 1550 nm.

Cloud type	N (cm^{-3})	\mathcal{L}_W (g/m^{-3})	V (km)
Cumulus	250	1.0	0.0280
Stratus	250	0.29	0.0626
Stratocumulus	250	0.15	0.0959
Altostratus	400	0.41	0.0369
Nimbostratus	200	0.65	0.0429
Cirrus	0.025	0.06405	64.66
Thin cirrus	0.5	3.128×10^{-4}	290.69

2) *Atmospheric Attenuation due to Geometrical Scattering:* Geometrical scattering is used to model the attenuation that is close to the surface of the Earth and is caused by fog or dense clouds. In this model, visibility (V_j), which is an important factor for determining geometrical scattering, can be modeled in terms of liquid water content (\mathcal{L}_{W_j}) and cloud number concentration (N_j) as [26]

$$V_j = \frac{1.002}{(\mathcal{L}_{W_j} N_j)^{0.6473}}. \quad (6)$$

These parameters are summarized in Table I for various cloud formations. In geometrical scattering, the attenuation can be expressed by using the Beer-Lambert law,

$$I_j^{(g)} = \exp(-\Theta_j L_j), \quad (7)$$

where L_j is the propagation distance, and Θ_j is the attenuation coefficient, which can be expressed as [27, Sect. (3)]

$$\Theta_j = \left(\frac{3.91}{V_j}\right) \left(\frac{\lambda}{550}\right)^{-\psi_j}, \quad (8)$$

TABLE II: List of Notations and Parameters

Parameter	Definition
D_G	Hard receiver aperture diameter (m)
\mathcal{K}	Set of GSs that are available for communication
L	Propagation distance
ζ	Zenith angle
θ	Elevation angle
v_r	Ground wind speed in rms
v_g	Ground wind speed (m/s)
h_E	Height of the GS above mean sea level (km)
h	Altitude
H	Altitude of the satellite (m)
h_0	Height of the GS above ground level (m)
ρ_c	Atmospheric correlation width
λ	Wavelength
α, β	Shape parameters of the EW fading
η	Fading severity parameter of the EW fading
k	Optical wave number
V	Visibility (km)
ψ	Particle size related coefficient
N	Cloud number concentration
Θ	Attenuation coefficient
\mathcal{L}_W	Liquid water content
σ_R^2	Rytov variance
C_n^2	Refractive index constant
σ_I^2	Scintillation index
γ_{th}	Predefined threshold for acceptable communication quality

where ψ is the particle size related coefficient given according to Kim's model as

$$\psi_j = \begin{cases} 1.6, & V_j > 50 \\ 1.3 & 6 < V_j < 50 \\ 0.16V_j + 0.34 & 1 < V_j < 6 \\ V - 0.5 & 0.5 < V_j < 1 \\ 0 & V_j < 0.5, \end{cases} \quad (9)$$

and the atmospheric attenuation $I_j^{(a)}$ for the j -th GS can be expressed as [18]

$$I_j^{(a)} = I_j^{(g)} I_j^{(m)} = \exp(-\sigma_j L_j) \exp\left(-\frac{\rho'}{\sin(\theta_j)}\right). \quad (10)$$

B. Turbulence Induced Fading Model

In this paper, the turbulence induced downlink channel experiences an exponentiated Weibull fading channel, where the corresponding probability density function (PDF) and cumulative distribution function (CDF) can be expressed as [28]

$$f_{I_j}^{(i)}(I) = \frac{\alpha_j \beta_j}{\eta_j} \left(\frac{I}{\eta_j}\right)^{\beta_j-1} \exp\left[-\left(\frac{I}{\eta_j}\right)^{\beta_j}\right] \times \left(1 - \exp\left[-\left(\frac{I}{\eta_j}\right)^{\beta_j}\right]\right)^{\alpha_j-1} \quad (11)$$

and

$$F_{I_j}^{(i)}(I) = \left(1 - \exp\left[-\left(\frac{I}{\eta_j}\right)^{\beta_j}\right]\right)^{\alpha_j}, \quad (12)$$

where α_j, β_j are the shape parameters and η_j is the scale parameter of the j -th GS. The expressions for α_j, β_j , and η_j can be expressed as [29]

$$\begin{aligned} \alpha_j &= \frac{7.220 \times \sigma_{I_j}^{2/3}}{\Gamma(2.487 \sigma_{I_j}^{2/6} - 0.104)}, \\ \beta_j &= 1.012 \left(\alpha \sigma_{I_j}^2\right)^{-13/25} + 0.142 \\ \eta_j &= \frac{1}{\alpha \Gamma(1 + 1/\beta_j) g_1(\alpha_j, \beta_j)}, \end{aligned} \quad (13)$$

where $g_1(\alpha_j, \beta_j)$ is the α and β dependent constant variable, which can be written as [29]

$$g_1(\alpha_j, \beta_j) = \sum_{k=0}^{\infty} \frac{(-1)^k \Gamma(\alpha_j)}{k! (k+1)^{1+1/\beta_j} \Gamma(\alpha_j - k)}, \quad (14)$$

and $\sigma_{I_j}^2$ denotes the scintillation index of the j -th GS, which can be given by [30, Sect. (12)]

$$\sigma_{I_j}^2 = \exp\left[\frac{0.49 \sigma_R^2}{(1 + 1.11 \sigma_{R_j}^{12/5})^{7/6}} + \frac{0.51 \sigma_{R_j}^2}{(1 + 0.69 \sigma_{R_j}^{12/5})^{5/6}}\right] - 1, \quad (15)$$

and the Rytov variance $\sigma_{R_j}^2$ can be expressed as [30, Sect. (12)]

$$\sigma_{R_j}^2 = 2.25 k^{7/6} \sec^{11/6}(\zeta_j) \int_{h_0}^H C_{n_j}^2(h) (h - h_0)^{5/6} dh, \quad (16)$$

where $k = \frac{2\pi}{\lambda}$ is the optical wave number, ζ_j is the zenith angle of the j -th GS, h_0 stands for the height of the GS above ground level, H is the altitude of the satellite, and $C_{n_j}^2(h)$ is the altitude (h) dependent refractive index constant, which can be written as [31]

$$C_{n_j}^2(h) = 8.148 \times 10^{-56} v_{r_j}^2 h^{10} e^{-h/1000} + 2.7 \times 10^{-16} e^{-h/1500} + C_0 e^{-h/100} m^{-2/3}, \quad (17)$$

where $v_{r_j} = \sqrt{v_{g_j}^2 + 30.69 v_{g_j} + 348.91}$ is the ground wind speed in rms, v_{g_j} is the ground wind speed in m/s for the j -th GS, and $C_0 = 1.7 \times 10^{-14}$ is the nominal value of the refractive index constant at ground level. Table II summarizes all notations and parameters.

C. Problem Formulation

This section formulates the GS selection strategy for the proposed setup. In what follows, the GS with the highest instantaneous SNR is selected to maximize the site diversity. Mathematically speaking, it can be formulated as

$$j^* = \arg \max_{1 \leq j \leq K} [\gamma_j], \quad (18)$$

where j^* is the selected GS index. By doing so, outage probability (P_{out}) can be minimized as

$$P_{\text{out}} = \Pr[\gamma \leq \gamma_{th}] = \Pr\left[\max_{1 \leq j \leq \mathcal{K}} (\gamma_j) \leq \gamma_{th}\right], \quad (19)$$

where γ_{th} is the predefined threshold for acceptable communication quality. Furthermore, ergodic capacity, which can assess the ergodic channel capacity, can be formulated as [32]

$$C_{\text{erg}} = \mathbb{E}\left[\log_2\left(1 + \max_{1 \leq j \leq \mathcal{K}} (\gamma_j)\right)\right], \quad (20)$$

where $\mathbb{E}[\cdot]$ is the expectation operation. It is important to note that it is almost impossible to find an exact ergodic capacity expression for the proposed scenario by using (20). Therefore, with the aid of Jensen's inequality, we propose two approximate ergodic capacity bounds as given here;

$$C_{\text{erg}}^{\text{B}_1} \approx \max_{1 \leq j \leq \mathcal{K}} \mathbb{E}[\log_2(1 + \gamma_j)], \quad (21a)$$

$$C_{\text{erg}}^{\text{B}_2} \approx \log_2\left(\mathbb{E}\left[1 + \max_{1 \leq j \leq \mathcal{K}} (\gamma_j)\right]\right), \quad (21b)$$

III. PERFORMANCE ANALYSIS

This section derives new closed-form outage probability and ergodic capacity expressions for the proposed system.

A. Outage Probability Analysis

Outage probability (OP) can be defined as the probability that the SNR will fall below a predefined threshold, γ_{th} , for acceptable communication quality. By substituting (12) into (19), with the aid of (18), the OP can be expressed as

$$P_{\text{out}} = \prod_{j=1}^{\mathcal{K}} \left(1 - \exp\left[-\left(\frac{\gamma_{th}}{(\eta_j I_j^{(a)})^2 \bar{\gamma}_j^{(t)}}\right)^{\beta_j/2}\right]\right)^{\alpha_j}, \quad (22)$$

where $\bar{\gamma}_j^{(t)} = \frac{P_S}{N_0} \mathbb{E}[(I_j^{(t)})^2]$ is the average SNR. By applying the Binomial theorem, and after a few manipulations, a tractable OP expression can be found as

$$P_{\text{out}} = \prod_{j=1}^{\mathcal{K}} \sum_{\rho=0}^{\infty} \binom{\alpha_j}{\rho} (-1)^\rho \exp\left[-\rho \left(\frac{\gamma_{th}}{(I_j^{(a)} \eta_j)^2 \bar{\gamma}_j^{(t)}}\right)^{\frac{\beta_j}{2}}\right]. \quad (23)$$

To gain further insights about the system behavior, the OP can be analyzed at high SNR. To do so, we first invoke the high SNR assumption of $\exp(-x/a) \approx 1 - x/a$ into (22) as

$$P_{\text{out}}^{\infty} = \prod_{j=1}^{\mathcal{K}} \left[1 - \left(\frac{\gamma_{th}}{(\eta_j I_j^{(a)})^2 \bar{\gamma}_j^{(t)}}\right)^{\alpha_j \beta_j/2}\right]. \quad (24)$$

Then, if we express $\bar{\gamma}_j^{(t)} = \kappa_j \bar{\gamma}$, where $\kappa_j|_{j=1}^{\mathcal{K}}$ is constant, after a few manipulations, the above expression can be written as

$$P_{\text{out}}^{\infty} = \prod_{j=1}^{\mathcal{K}} \left[1 - \left(\frac{1}{(\eta_j I_j^{(a)})^2 \kappa_j}\right)^{\alpha_j \beta_j/2}\right] \left(\frac{\gamma_{th}}{\bar{\gamma}}\right)^{\sum_{j=1}^{\mathcal{K}} \alpha_j \beta_j/2}, \quad (25)$$

TABLE III: Outage probabilities for ground level deployment and high ground windy weather deployment scenarios

Scenario	ζ	N	L_W	Outage probability
Case 1	40°	0.5	3.128×10^{-4}	0.8166
	30°	0.5	3.128×10^{-4}	0.1619
	15°	0.5	3.128×10^{-4}	5.583×10^{-4}
	0°	0.5	3.128×10^{-4}	2.165×10^{-5}
Case 2	40°	0.5	3.128×10^{-4}	0.0986
	30°	0.5	3.128×10^{-4}	2.314×10^{-4}
	15°	0.5	3.128×10^{-4}	2.27×10^{-9}
	0°	0.5	3.128×10^{-4}	1.28×10^{-11}

and the site diversity gain can be obtained as $\mathcal{G}_d = \sum_{j=1}^{\mathcal{K}} \alpha_j \beta_j/2$. Furthermore, in this section, we propose two different practical deployment scenarios and investigate the OP performance of the proposed setup when there are $\mathcal{K} = 20$ set of GSs that are available for communication.

1) *Case 1 - Ground level deployment scenario:* In the first setup, we assume that all GSs are deployed at the ground level ($h_0 = h_E = 0$), having $v_g = 2.8$ m/s nominal ground wind speed. Under these assumptions, and assuming $\bar{\gamma} = 24$ dB average SNR, the OPs that are required for acceptable communication quality ($\gamma_{th} = 7$ dB) can be obtained as given in Case 1, Table III.

2) *Case 2 - High ground windy weather deployment scenario:* In the second setup, we consider that all GSs are deployed at high ground and are heavily affected by the windy weather. In this scenario, all GSs are deployed at $h_0 = 1000$ m from the ground level and $h_E = 1.2$ km from the mean sea level, where the wind is blowing at $v_g = 11.176$ m/s speed. Assuming that the average SNR is $\bar{\gamma} = 24$ dB, the OPs that are required for acceptable communication quality can be summarized in Case 2, Table III.

Table III shows the OP results for thin cirrus cloud formations, when the altitude of the satellite is chosen as 500 km. We can see from the table that, even though the wind speed increases in the high ground deployment, the overall OP performance of the proposed system enhances as both atmospheric turbulence and atmospheric attenuation effects reduces due to lower propagation distance. Furthermore, increasing the zenith angle shows that the GSs are affected by the attenuation and atmospheric turbulence at higher levels. Thereby, keeping the zenith angle small, can boost the overall performance and can enhance the overall site diversity gain as can be observed from Fig. 2.

B. Ergodic Capacity Analysis

1) *First Approximate Bound on the Ergodic Capacity:* Ergodic capacity, expressed in bits/channel in use, can be defined with the aid of (21a) as

$$C_{\text{erg}}^{\text{B}_1} = \log_2(e) \max_{1 \leq j \leq \mathcal{K}} \left\{ \int_0^{\infty} \frac{1}{1+\gamma} \bar{F}_{\gamma_j}(\gamma) d\gamma \right\}, \quad (26)$$

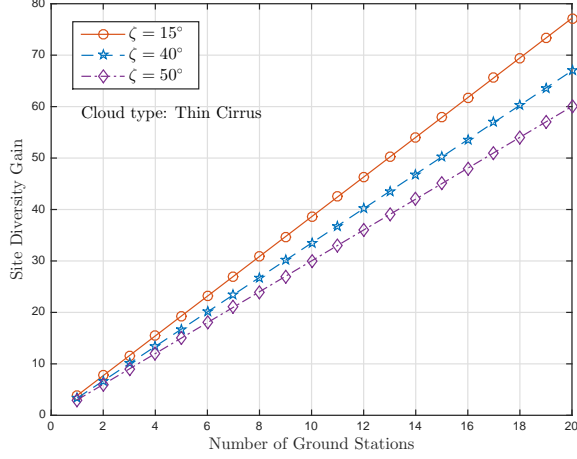


Fig. 2: Site diversity gain vs number of ground stations for the ground level deployment scenario.

where $\bar{F}_{\gamma_j}(\gamma) = 1 - F_{\gamma_j}(\gamma)$ is the complementary CDF of γ_j , which can be given as

$$\bar{F}_{\gamma_j}(\gamma) = \sum_{\rho=1}^{\infty} \binom{\alpha_j}{\rho} (-1)^{\rho+1} \exp \left[-\rho \left(\frac{\gamma}{(\eta_j I_j^{(a)})^2 \bar{\gamma}_j^{(t)}} \right)^{\frac{\beta_j}{2}} \right], \quad (27)$$

then, by invoking $\bar{F}_{\gamma_j}(\gamma)$ into (26), C_{erg} can be expressed as

$$C_{\text{erg}}^{\text{B}_1} = \log_2(e) \max_{1 \leq j \leq K} \left\{ \sum_{\rho=1}^{\infty} \binom{\alpha_j}{\rho} (-1)^{\rho+1} \int_0^{\infty} \frac{1}{1+\gamma} \times \exp \left[-\rho \left(\frac{\gamma}{(\eta_j I_j^{(a)})^2 \bar{\gamma}_j^{(t)}} \right)^{\frac{\beta_j}{2}} \right] d\gamma \right\}. \quad (28)$$

To find the closed-form solution of the above integral, we first use the identity of $\frac{1}{1+\gamma} = G_{1,1}^{1,1} \left[\gamma \begin{smallmatrix} 0 \\ 0 \end{smallmatrix} \right]$, and we can express C_{erg} as

$$C_{\text{erg}}^{\text{B}_1} = \log_2(e) \max_{1 \leq j \leq K} \left\{ \sum_{\rho=1}^{\infty} \binom{\alpha_j}{\rho} (-1)^{\rho+1} \int_0^{\infty} G_{1,1}^{1,1} \left[\gamma \begin{smallmatrix} 0 \\ 0 \end{smallmatrix} \right] \times \exp \left[-\rho \left(\frac{\gamma}{\Omega_j} \right)^{\frac{\beta_j}{2}} \right] d\gamma \right\}, \quad (29)$$

where $\Omega_j = (I_j^{(a)} \eta_j)^2 \bar{\gamma}_j^{(t)}$ and $G_{c,d}^{a,b} \left[\cdot \begin{smallmatrix} \cdot \\ \cdot \end{smallmatrix} \right]$ denotes the Meijer-G function [33, eqn. 07.34.02.0001.01]. By changing variables in the above integration as $\chi = \rho \left(\frac{\gamma}{\Omega_j} \right)^{\frac{\beta_j}{2}}$ and by using the identity of $\exp(-x) = G_{0,1}^{1,0} \left[x \begin{smallmatrix} - \\ 0 \end{smallmatrix} \right]$, the ergodic capacity can be

written as

$$C_{\text{erg}}^{\text{B}_1} = \log_2(e) \max_{1 \leq j \leq K} \left\{ \sum_{\rho=1}^{\infty} \binom{\alpha_j}{\rho} (-1)^{\rho+1} \rho^{\frac{\beta_j}{2}} \left(\frac{2\Omega_j}{\beta_j} \right) \times \int_0^{\infty} \chi^{\frac{2}{\beta_j}-1} G_{1,1}^{1,1} \left[\Omega_j \left(\frac{\chi}{\rho} \right)^{\frac{2}{\beta_j}} \begin{smallmatrix} 0 \\ 0 \end{smallmatrix} \right] G_{0,1}^{1,0} \left[\chi \begin{smallmatrix} - \\ 0 \end{smallmatrix} \right] d\chi \right\}, \quad (30)$$

and with the aid of [33, eqn. 07.34.21.0012.01], the closed form solution of the above expression can be obtained as

$$C_{\text{erg}}^{\text{B}_1} = \log_2(e) \max_{1 \leq j \leq K} \left\{ \sum_{\rho=1}^{\infty} \binom{\alpha_j}{\rho} (-1)^{\rho+1} \rho^{\frac{\beta_j}{2}} \left(\frac{2\Omega_j}{\beta_j} \right) \times H_{2,1}^{1,2} \left[\Omega_j \rho^{\frac{\beta_j}{2}} \begin{smallmatrix} (0,1), (1-\frac{2}{\beta_j}, \frac{2}{\beta_j}) \\ (0,1) \end{smallmatrix} \right] \right\}. \quad (31)$$

where $H_{p,q}^{m,n} \left[\cdot \begin{smallmatrix} \cdot \\ \cdot \end{smallmatrix} \right]$ denotes the Fox H-function [34].

2) *Second Approximate Bound on the Ergodic Capacity:* Another tight bound on the ergodic capacity can be obtained by using (21b). First, recall that

$$C_{\text{erg}}^{\text{B}_2} \approx \log_2 \left(1 + \mathbb{E} \left[\underbrace{\max_{1 \leq j \leq K} (\gamma_j)}_{\gamma} \right] \right). \quad (32)$$

Thereafter, $\mathbb{E}[\gamma]$ can be expressed as

$$\mathbb{E}[\gamma] = \int_0^{\infty} (1 - F_{\gamma}(\gamma)) d\gamma, \quad (33)$$

where $F_{\gamma}(\gamma)$ can be obtained very similarly to (23) after changing γ_{th} with γ , and it can be approximately expressed as

$$F_{\gamma}(\gamma) \approx \sum_{\rho=0}^{\infty} \binom{K\alpha}{\rho} (-1)^{\rho} \exp \left[-\rho \left(\frac{\gamma_{th}}{(I^{(a)} \eta)^2 \bar{\gamma}^{(t)}} \right)^{\frac{\beta}{2}} \right]. \quad (34)$$

By substituting (34) into (33), and after few manipulations, $\mathbb{E}[\gamma]$ can be obtained as

$$\mathbb{E}[\gamma] = \sum_{\rho=1}^{\infty} \binom{K\alpha}{\rho} (-1)^{\rho+1} \rho^{-2/\beta} \bar{\gamma}^{(t)} (I^{(a)} \eta)^2 \Gamma(1 + 2/\beta). \quad (35)$$

Finally, substituting (35) into (32), $C_{\text{erg}}^{\text{B}_2}$ can be easily obtained.

C. Aperture Averaging

In downlink optical SatCom, the impact of scintillation can be great enough to limit the performance of GS receivers. To compensate for the impact of scintillation, an important enabler is aperture averaging. In downlink communication, aperture averaging takes place especially when the atmospheric correlation width ρ_{c_j} , which describes the effective diameter of the j -th aperture, is lower than the aperture diameter of the j -th GS (D_{G_j}), i.e. $\rho_{c_j} < D_{G_j}$. In this case, scintillation is spatially averaged over the aperture to reduce

TABLE IV: List of Parameters and Values

Parameters	Values
\mathcal{K}	10, 20
ζ	15°, 40°, 50°
λ	1.55 nm
H	5×10^5 m
h_0	0 m, 1000 m
h_E	0 km, 1.2 km
v_g	2.8 m/s, 11.176 m/s
γ_{th}	7 dB
C_0	1.7×10^{-14}

the adverse effects of scintillation. For the proposed setup, ρ_{c_j} can be calculated as [30, Sect. (12)]

$$\rho_{c_j} \approx \sqrt{\frac{45 \times 10^3 \sec(\zeta_j)}{k}}, \quad \sigma_{R_j}^2 < 1, \quad 0 \leq \zeta_j < 50, \quad (36)$$

where ρ_{c_j} represents the diameter of the point-like aperture for the GS. For example, when $\zeta_j = 40^\circ$, $\rho_{c_j} \approx 1.204$ cm shows the point-like aperture size for the optical downlink SatCom operating at $\lambda = 1.55$ nm wavelength. In aperture averaging, the aperture diameter dependent scintillation index can be expressed as [30, Sect. (12)]

$$\sigma_{I_j}^2 = 8.7k^{7/6}(H - h_0)^{5/6} \sec^{11/6}(\zeta_j) \times \Re \left\{ \int_{h_0}^H C_n^2(h) \left[\left(\frac{kD_G^2}{16L} + i \frac{h - h_0}{H - h_0} \right)^{5/6} - \left(\frac{kD_{G_j}^2}{16L_j} \right)^{5/6} \right] \right\}, \quad (37)$$

where $\Re\{\cdot\}$ represents the real-valued terms. For example, considering $\zeta_j = 40^\circ$, $H = 5 \times 10^5$ m, and thin cirrus cloud formations for the ground level deployment scenario, $D_g = 20$ cm aperture size can boost the overall outage performance from 6.884×10^{-7} to 3.441×10^{-9} at 30 dB average SNR.

IV. NUMERICAL RESULTS

In this section, the theoretical results are first verified by a set of simulations. Then, the ground level deployment scenario is compared with the high ground windy weather deployment scenario in terms of outage probability and ergodic capacity. Finally, aperture averaging is illustrated in terms of outage probability, and important design guidelines are outlined for practical downlink laser SatComs.

In all figures, the parameters are set as $\alpha_j = \alpha$, $\beta_j = \beta$, $\eta_j = \eta$, $I_j^{(a)} = I^{(a)}$, $I_j^{(t)} = I^{(t)}$, $\zeta_j = \zeta$, $\psi_j = \psi$, $C_{n_j}^2(h) = C_n^2(h)$, $\sigma_{I_j}^2 = \sigma_I^2$, $\sigma_{R_j}^2 = \sigma_R^2$ for notational brevity, without losing generality. Furthermore, in the ground level deployment scenario, the parameters are set as $h_0 = h_E = 0$ m, $v_g = 2.8$ m/s, whereas to demonstrate the high ground windy weather scenario, the parameters are set as $h_0 = 1000$ m, $h_E = 1.2$ km, and $v_g = 11.176$ m/s. Finally, the SNR threshold is set to $\gamma_{th} = 7$ dB, and two different cloud forms, cirrus and thin cirrus, are used in the simulations together with three different ζ angles: $\zeta = 15^\circ, 40^\circ$ and 50° . All these parameters and values are illustrated in Table IV.

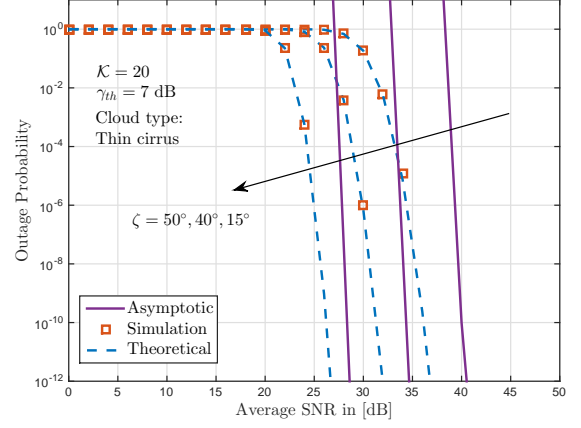


Fig. 3: Outage probability performance of the proposed scheme for the ground level deployment scenario.

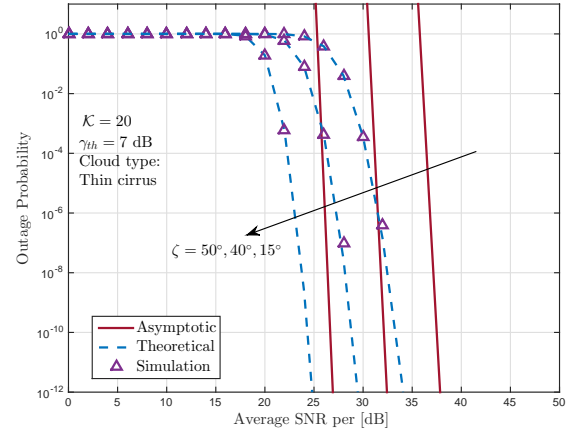


Fig. 4: Outage probability performance of the proposed scheme for the high ground windy weather deployment scenario.

A. Verifications of the Theoretical Expressions

Here we verify the theoretical results with the simulations. As we can see in Fig. 3 and 4, the theoretical outage probability results, which are shown with dashed lines, are in good agreement with the marker symbols, which are generated by the simulations. Furthermore, both figures show that the overall outage performance of the proposed scheme can be enhanced remarkably by increasing the ζ angle as expected. Finally, asymptotic curves, which are depicted with solid lines, show the overall site diversity gain, which is close to $\mathcal{G}_d = 10\alpha\beta \approx 70$ at both figures.

Fig. 5, on the other hand, illustrates the ergodic capacity performance of the proposed scheme for the high ground

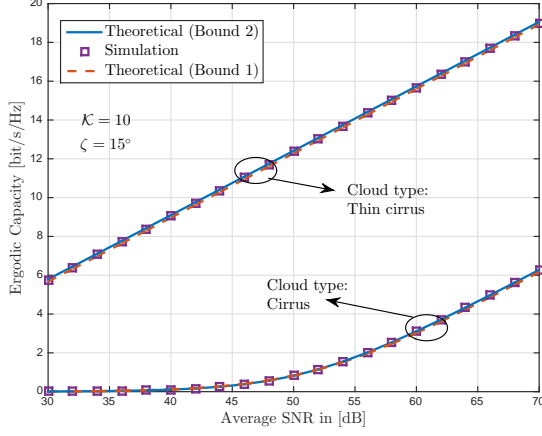


Fig. 5: Ergodic capacity performance of the proposed scheme for the high ground windy weather deployment scenario.

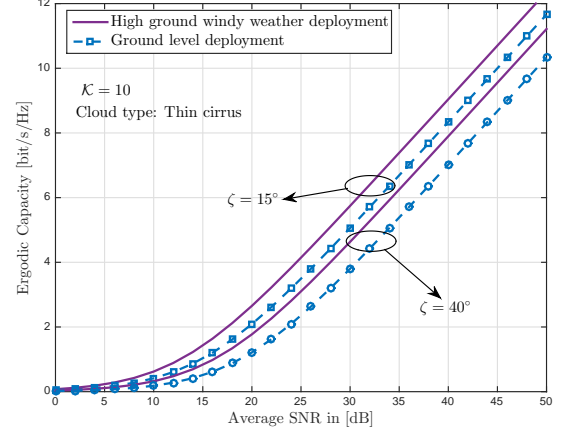


Fig. 7: Comparison of ground level deployment with high ground windy weather deployment in terms of ergodic capacity.

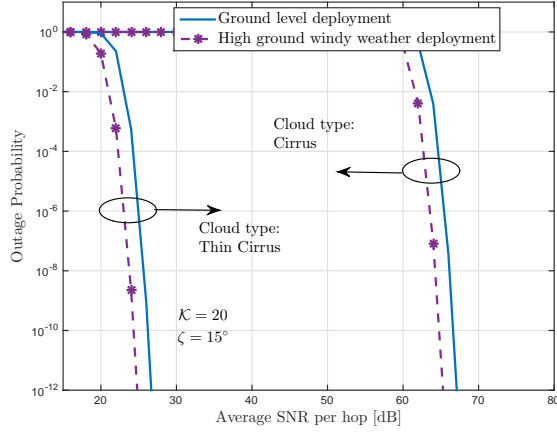


Fig. 6: Comparison of ground level deployment with high ground windy weather deployment in terms of outage probability.

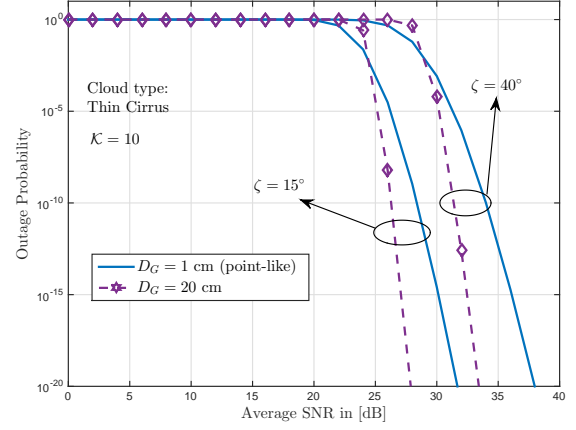


Fig. 8: The impact of aperture averaging on the ground level deployment scenario in terms of outage probability.

windy weather deployment scenario⁵. As we can see in the figure, theoretical bound 2, which is shown with solid lines, provides a tight upper bound, whereas theoretical bound 1, which are indicated with the dashed lines behaves like a tight lower bound with the marker symbols, which are the results of the simulations. Furthermore, thin cloud formations can bring up to 11 bit/s/Hz capacity gain at 50 dB average SNR as the atmospheric attenuation increases due to cirrus cloud formations, and results in losses on the ergodic capacity performance of the proposed scheme.

⁵Theoretical results that are evaluated by using bound 1 (shown with dashed lines) can be easily obtained by using Fox-H function in well-known software programs like MATHEMATICA or MATLAB. However, in a few cases, the Fox-H function may not work properly due to fractional fading severity values. For this reason, numerical integrations are used to verify the correctness of the first bound in certain cases.

B. Comparison of High Ground Windy Weather Deployment and Ground Level Deployment Scenarios

Next, the ground level deployment scenario is compared with the high ground windy weather deployment scenario in terms of outage probability and ergodic capacity. Fig. 6 compares both schemes in terms of outage probability. As we can see in the figure, the high ground windy weather scenario outperforms the ground level counterpart both at thin cirrus and cirrus cloud formations, when $\zeta = 15^\circ$. Similarly, Fig. 7 shows the ergodic capacity performance of both scenarios at $\zeta = 15^\circ$ and 40° . As expected, the high ground windy weather deployment scenario outperforms its counterpart. Interestingly, both figures show that placing the GSs at higher ground enhances the overall performance as it reduces the overall atmospheric attenuation even in windy weather.

C. Impact of Aperture Averaging

This section shows the impact of aperture averaging for the ground level deployment scenario in terms of outage

probability. Fig. 8 shows that increasing the receiver aperture diameter up to 20 cm increases the site diversity gain and enhances the overall performance depending on the zenith angle and weather conditions. Also, interestingly, choosing the optimum zenith angle can yield a higher performance gain than aperture averaging.

D. Design Guidelines

Finally, we provide some important design guidelines that can be helpful in the design of downlink laser SatCom.

- The simulations have shown that placing the GS to higher ground reduces the adverse atmospheric conditions and enhances the overall performance. So, the altitude of the GSs is of utmost importance in the design of downlink laser SatComs.
- The zenith angle has a direct impact on the design of downlink laser SatComs as the effect of atmospheric turbulence is much lower when the zenith angle is a small value. For this reason, the zenith angle should be taken into consideration in the design of downlink laser SatCom.
- Aperture averaging can be an important enabler for enhancing the overall performance of the downlink laser SatComs, especially in the presence of adverse weather conditions, and when the zenith angle is higher than $\zeta = 30^\circ$.
- The simulations have shown that at least 10^{-10} outage probability can be achieved at 30 dB when a set of 20 GSs is used. This shows that creating site diversity through GS selection can be of utmost importance in downlink laser SatComs to enhance the overall performance.

V. CONCLUSION

This paper has focused on downlink laser SatComs, where the best GS is selected from among a set of \mathcal{K} candidates to provide fully reliable connectivity and maximum site diversity. For the proposed structure, outage probability and ergodic capacity expressions were derived and asymptotic outage probability was conducted to provide the overall site diversity gain. Furthermore, we considered two different ground station deployment scenarios and investigated the impact of aperture averaging in terms of outage probability. Finally, important system design guidelines were provided to help in the design of downlink laser SatComs. The results have shown that the altitude of the GS and the zenith angle are of utmost importance in downlink laser SatComs.

REFERENCES

- [1] D. R. Cheruku, *Satellite Communication*. I.K. International Publishing House Pvt Ltd, Delhi, India, 2010.
- [2] P. Timothy, W. Bostian, and J. E. Allnutt, *Satellite Communication*. John Wiley & Sons, New York, USA, 2003.
- [3] S. L. Kota, K. Pahlavan, and P. A. Leppänen, *Broadband Satellite Communications for Internet Access*. Kluwer Academic Publishers, Norwell, USA, 2003.
- [4] "Starlink," <https://www.starlink.com>, Accessed: 2020-08-20.
- [5] "Oneweb," <http://www.oneweb.world>, Accessed: 2020-08-20.
- [6] H. Kaushal and G. Kaddoum, "Optical communication in space: Challenges and mitigation techniques," *IEEE Communications Surveys & Tutorials*, vol. 19, no. 1, pp. 57–96, Aug. 2016.
- [7] ITU-R, "Prediction methods required for the design of Earth-space systems operating between 20 THz and 375 THz," International Telecommunication Union, Recommendation P.1622, Apr. 2003.
- [8] A. N. Ince, *Digital Satellite Communications Systems and Technologies: Military and Civil Applications*. Springer Science & Business Media, Sep. 2012, vol. 186.
- [9] D. Giggenbach, B. Epple, J. Horwath, and F. Moll, "Optical satellite downlinks to optical ground stations and high-altitude platforms," in *Advances in Mobile and Wireless Communications*. Springer, Jul. 2008, pp. 331–349.
- [10] V. V. Mai and H. Kim, "Mitigation of effects of angle-of-arrival fluctuation and pointing error on airborne free-space optical systems," in *Optical Fiber Communication Conference*, Mar. 2019, pp. W2A–40.
- [11] D. Agarwal and A. Bansal, "Unified error performance of a multihop DF-FSO network with aperture averaging," *IEEE/OSA Journal of Optical Communications and Networking*, vol. 11, no. 3, pp. 95–106, Mar. 2019.
- [12] C. Fuchs and F. Moll, "Ground station network optimization for space-to-ground optical communication links," *IEEE/OSA Journal of Optical Communications and Networking*, vol. 7, no. 12, pp. 1148–1159, Dec. 2015.
- [13] M. S. Net, I. Del Portillo, E. Crawley, and B. Cameron, "Approximation methods for estimating the availability of optical ground networks," *Journal of Optical Communications and Networking*, vol. 8, no. 10, pp. 800–812, Oct. 2016.
- [14] N. K. Lyras, C. N. Efrem, C. I. Kourogiorgas, and A. D. Panagopoulos, "Optimum monthly based selection of ground stations for optical satellite networks," *IEEE Communications Letters*, vol. 22, no. 6, pp. 1192–1195, Jun. 2018.
- [15] S. Gong, H. Shen, K. Zhao, R. Wang, X. Zhang, T. De Cola, and J. A. Fraier, "Network availability maximization for free-space optical satellite communications," *IEEE Wireless Communications Letters*, vol. 9, no. 3, pp. 411–415, Mar. 2019.
- [16] P. Gopal, V. K. Jain, and S. Kar, "Performance improvement of FSO satellite downlink using aperture averaging and receiver spatial diversity," *IET Optoelectronics*, vol. 10, no. 4, pp. 119–127, Jul. 2016.
- [17] K. Li, J. Ma, A. Belmonte, L. Tan, and S. Yu, "Performance analysis of satellite-to-ground downlink optical communications with spatial diversity over Gamma-Gamma atmospheric turbulence," *Optical Engineering*, vol. 54, no. 12, pp. 7575–7585, Aug. 2015.
- [18] S. Johari and V. Sundharam, "Performance analysis of IM/DD vs. heterodyne detection techniques of an earth-satellite FSO link for next generation wireless communication," in *Malaysia International Conference on Communications (MICC)*, Nov. 2017, pp. 191–196.
- [19] A. Viswanath, V. K. Jain, and S. Kar, "Analysis of earth-to-satellite free-space optical link performance in the presence of turbulence, beam-wander induced pointing error and weather conditions for different intensity modulation schemes," *IET Communications*, vol. 9, no. 18, pp. 2253–2258, Dec. 2015.
- [20] N. Alshaer, T. Ismail, and M. E. Nasr, "Performance evaluation and security analysis of ground-to-satellite FSO system with CV-QKD protocol," *IET Communications*, vol. 14, no. 10, pp. 1534–1542, Jun. 2020.
- [21] N. Alshaer, T. Ismail, H. Seleem, and M. E. Nasr, "Analysis of beam wander and scintillation in ground-to-satellite FSO system with DPSK," in *Novel Intelligent and Leading Emerging Sciences Conference (NILES)*, vol. 1, Nov. 2019, pp. 5–8.
- [22] H. D. Le, V. V. Mai, C. T. Nguyen, and A. T. Pham, "Throughput analysis of incremental redundancy hybrid ARQ for FSO-based satellite systems," in *IEEE 90th Vehicular Technology Conference (VTC2019-Fall)*, Nov. 2019, pp. 1–5.
- [23] E. Illi, F. El Bouanani, F. Ayoub, and M.-S. Alouini, "A PHY layer security analysis of a hybrid high throughput satellite with an optical feeder link," *IEEE Open Journal of the Communications Society*, vol. 1, pp. 713 – 731, May 2020.
- [24] E. Zedini, A. Kammoun, and M.-S. Alouini, "Performance of multibeam very high throughput satellite systems based on FSO feeder links with HPA nonlinearity," *IEEE Transactions on Wireless Communications*, vol. 19, no. 9, pp. 5908 – 5923, Jun. 2020.
- [25] E. Erdogan, "Joint user and relay selection for relay-aided RF/FSO systems over exponentiated Weibull fading channels," *Optics Communications*, vol. 436, pp. 209–215, Apr. 2019.
- [26] M. S. Awan, E. Leitgeb, B. Hillbrand, F. Nadeem, M. Khan *et al.*, "Cloud attenuations for free-space optical links," in *International Workshop on Satellite and Space Communications*, Sep. 2009, pp. 274–278.

- [27] Z. Ghassemlooy, W. Popoola, and S. Rajbhandari, *Optical Wireless Communications: System and Channel Modelling with Matlab®*. CRC Press, 2019.
- [28] R. Barrios and F. Dios, "Exponentiated Weibull distribution family under aperture averaging for Gaussian beam waves," *Optical Express*, vol. 20, no. 12, pp. 13 055–13 064, May 2012.
- [29] R. A. Barrios, "Exponentiated Weibull fading channel model in free-space optical communications under atmospheric turbulence," Ph.D. dissertation, Universitat Politècnica de Catalunya (UPC), May 2013.
- [30] L. Andrews and R. Phillips, *Laser Beam Propagation Through Random Media*, ser. SPIE Press monograph. SPIE Press, 2005.
- [31] ITU-R, "Propagation data required for the design of Earth-space systems operating between 20 THz and 375 THz," International Telecommunication Union, Recommendation P.1621-1, Jul. 2015.
- [32] J. Choi and B. L. Evans, "Analysis of ergodic rate for transmit antenna selection in low-resolution ADC systems," *IEEE Transactions on Vehicular Technology*, vol. 68, no. 1, pp. 952–956, Oct. 2018.
- [33] "From Wolfram Research: The mathematical functions site," <http://functions.wolfram.com>, Accessed: 2020-06-18.
- [34] A. M. Mathai, R. K. Saxena, and H. J. Haubold, *The H-Function: Theory and Applications*. Springer Science & Business Media, 2009.